

# Magnetic properties of a disordered substitutional alloy—Heisenberg model

H. Dvey-Aharon\* and M. Fibich

Physics Department, Technion-Israel Institute of Technology, Haifa, Israel

(Received 18 March 1976; revised manuscript received 31 March 1977)

The magnetic properties of a disordered  $A_xB_{1-x}$  substitutional alloy, with  $A$ - $A$  interactions only, are analyzed in terms of a Heisenberg-type Hamiltonian. The critical temperature  $T_c(x)$  and the critical concentration  $x_c$ , below which no bulk ferromagnetism exists, are calculated for various ratios of the second- to first-nearest-neighbors interactions. Results for  $x_c$  are shown to agree with the critical percolation concentration for each case. The dispersion relation and the density of states of the spin-wave spectrum are calculated and compared with those obtained by other techniques and for different types of disorder. For  $x < x_c$ , spin-wave excitations exist for wave numbers  $k$  above a certain lower bound  $k_c(x)$ . The inverse of  $k_c$  is interpreted as the linear dimension of the largest magnetic cluster that the system can sustain at  $x < x_c$ . Results are compared with those obtained by percolation methods. The magnetization and the specific heat are also calculated and compared with experimental data.

## I. INTRODUCTION

The magnetic properties of random alloys  $A_xB_{1-x}$ , in which the  $A$  (magnetic) and  $B$  (nonmagnetic) atoms are distributed randomly on a regular lattice, have been thoroughly investigated during the last fifteen years. In the earlier works, attempts have been made to calculate the ferromagnetic transition temperature  $T_c(x)$  and the critical concentration  $x_c$ , below which no bulk ferromagnetism can exist. Brout<sup>1</sup> has argued that, for long-range exchange interactions,  $T_c$  increases linearly with  $x$  and extrapolates to zero at  $x=0$  (i.e., no finite  $x_c$  exists). For short-range interactions, however, he conjectured that a finite critical concentration  $x_c$  exists. This kind of behavior of  $T_c(x)$  was found by Sato *et al.*<sup>2</sup> for an Ising model with nearest-neighbors (nn) interactions only, by Smart<sup>3</sup> for a classical Heisenberg ferromagnet, and by Elliot and Heap<sup>4,5</sup> for a spin- $\frac{1}{2}$  system. As for  $x_c$ , it was found to be strongly dependent on lattice coordination number  $[(z-1)^{-1}$  in Refs. 2 and 3]. Charap<sup>6</sup> improved Smart's result<sup>3</sup> by also taking into account the fluctuations in the molecular field seen by any first-shell magnetic atom. Relating  $x_c$  to lattice percolation properties was first suggested by de Gennes *et al.*<sup>7,8</sup> and later used by several authors.<sup>9-13</sup>

Another avenue of approach to the problem of disordered ferromagnetic alloys is to treat the dynamics of the disordered spin system, such as the spin-wave excitations that the system can sustain. Murray<sup>14</sup> has used a variational method to calculate the spin-wave energy of a Heisenberg ferromagnet. In the long-wavelength limit ( $k \rightarrow 0$ ), she found an upper bound to the excitation energy which has the form  $\phi(x)k^2$  where  $\phi(x)$  is a nearly linear function of  $x$  which vanishes at  $x_c$  [0.44 for a single cubic (sc) lattice]. Murray's variational principle was

recently criticized by Kumar and Harris,<sup>15</sup> mainly for two reasons. First, it allows  $\phi(x)$  to be negative even though the system orders ferromagnetically. Secondly, a finite bound for  $\phi(x)$  can be found for  $x < x_c$  although obviously no long-wavelength spin waves exist. Following Murray's work, a somewhat better estimate of  $\phi(x)$  and the corresponding  $x_c$  was found by Kaneyoshi,<sup>16</sup> and later on by Edwards and Jones.<sup>17</sup> They obtained an infinite-series expansion in powers of  $x$  and  $1-x$ , but were able, however, to calculate exactly only the first few terms of that series.

This difficulty can, in principle, be avoided if one obtains a Dyson equation for the spin-spin Green's function.<sup>18-20</sup> That last equation is then solved either by a  $T$ -matrix calculation<sup>18</sup> (with a truncation scheme for  $T$  based on cutting off the influence of all but the nearest neighborhood of a single atom<sup>21</sup>), or by coherent-potential approximation<sup>19,22</sup> (CPA). These techniques are used to derive the spin-wave density of states and dispersion relations, as well as  $T_c(x)$  and  $x_c$ .<sup>18</sup>

In the present work the  $A_xB_{1-x}$  ferromagnet, governed by a Heisenberg Hamiltonian, is examined. We derive, within the framework of the spin-wave approximation, a Dyson equation for the configurationally averaged Green's function  $G(\vec{k}, \omega)$ . To this end we first derive an equation for the unaveraged Green's function. This equation is then decoupled using a quadratic approximation which is described in Secs. II and III. We thus obtain a compact expression for  $\bar{G}$  which is then utilized to calculate the system's properties. In Sec. IV,  $T_c(x)$  and  $x_c$  are derived for the three cubic lattices and for nn and second-nn interactions. For positive nn and second-nn interaction all  $T_c(x)$  graphs, when plotted against the reduced concentration  $(x-x_c)/(1-x_c)$ , fall on a single universal graph. The critical concentration  $x_c$  agreed in all

cases quite well with the relevant critical percolation concentration

In Sec. V the response function is calculated and shown to fit quite well the very accurate "moment calculation" results of Nickel.<sup>23</sup> The response function is directly used to derive the dispersion relation and the density of states of the spin-wave excitations. These are also compared to CPA calculations of Harris *et al.*<sup>20</sup> and of Theumann and Tahir-Kheli.<sup>22</sup> For  $x < x_c$  the spin-wave excitations are shown to be physical for  $k > k_c(x)$  only. This limiting wave number  $k_c(x)$  may be interpreted as a measure of the inverse linear dimension  $l(x)$  of the largest cluster which can exist at  $x < x_c$ .

The size of the largest cluster  $l^3(x)$  is shown to diverge near the critical concentration as  $|x - x_c|^{-\delta}$  with  $\delta = 1.5$  close to the value 1.69 obtained by percolation-theory methods.<sup>11</sup>

In Sec. VI the magnetization  $\sigma(T)$  is derived, for various values of  $x$ , and compared with experimental data. The thermal demagnetization is shown to obey an  $a(x)T^{3/2}$  law, where  $a(x)$  is a rapidly decreasing function of  $x$ .  $a(x)$  is shown to agree with values deduced from experimental data in various systems. Finally we derive the specific heat  $C_v(x, T)$  and show how these results may be used to explain the anomalous peak near the critical concentration in some magnetic alloys.

## II. DERIVATION OF A CONFIGURATIONALLY AVERAGED GREEN'S FUNCTION

The system consists of random A-B alloy in an external field  $H$ . A spin  $\tilde{S}$  is associated with each A-type atom. We assume a Heisenberg-type interaction between these randomly distributed spins.

Hence, the Hamiltonian of the system is

$$\mathcal{H} = g\mu_B H \sum_{\alpha} S_{\alpha}^z - \sum_{\alpha, \beta} J_{\alpha\beta} \tilde{S}_{\alpha} \cdot \tilde{S}_{\beta}. \quad (2.1)$$

Here  $\tilde{S} \equiv \xi_{\alpha} \tilde{S}_{\alpha}$  where  $\tilde{S}_{\alpha}$  is the spin on site  $\alpha$  and  $\xi_{\alpha}$  take the value one if site  $\alpha$  is occupied by an A-type atom and zero otherwise.  $J_{\alpha\beta}$  is assumed to be a function of  $|\tilde{r}_{\alpha} - \tilde{r}_{\beta}|$  only, independent of local environment, so that  $J_{\alpha\beta} \equiv J_i$  if sites  $\alpha$  and  $\beta$  are neighbors of order  $i$ .

Transforming to wave-vector variables

$$J_{\alpha\beta} = N^{-1} \sum_{\mathbf{k}} J_{\mathbf{k}} e^{i\mathbf{k} \cdot (\tilde{r}_{\alpha} - \tilde{r}_{\beta})},$$

$$S_{\alpha}^{\mu} = \sum_{\mathbf{k}} S_{\mathbf{k}}^{\mu} e^{i\mathbf{k} \cdot \tilde{r}_{\alpha}}, \quad \mu = x, y, z, \pm,$$

we obtain

$$\mathcal{H} = Ng\mu_B HS_{\alpha}^z - N \sum_{\mathbf{k}} J_{\mathbf{k}} (S_{\mathbf{k}}^x S_{-\mathbf{k}}^x + S_{\mathbf{k}}^y S_{-\mathbf{k}}^y). \quad (2.2)$$

We then define the usual time-dependent Green's function,

$$G_{\mathbf{k}, \mathbf{k}'} = i\theta(t) \langle [S_{\mathbf{k}}^z(t), S_{\mathbf{k}'}^z(0)] \rangle \\ \equiv \langle \langle S_{\mathbf{k}}^z(t); S_{\mathbf{k}'}^z(0) \rangle \rangle. \quad (2.3)$$

We note that  $G_{\mathbf{k}, \mathbf{k}'}$  takes into account spin-spin correlation of A-type atoms only. The equation of motion of  $G_{\mathbf{k}, \mathbf{k}'}$  is

$$i \frac{\partial}{\partial t} G_{\mathbf{k}, \mathbf{k}'} = -2 \langle S_{\mathbf{k}-\mathbf{k}'}^z \rangle \delta(t) + g\mu_B H G_{\mathbf{k}, \mathbf{k}'} \\ + 2 \sum_{\mathbf{k}''} (J_{\mathbf{k}'', -} - J_{\mathbf{k}', -\mathbf{k}''}) \langle \langle S_{\mathbf{k}-\mathbf{k}'', -}^z(t); S_{\mathbf{k}'}^z(0) \rangle \rangle. \quad (2.4)$$

We now use the usual spin-wave approximation:

$$\langle \langle S_{\mathbf{k}-\mathbf{k}'', -}^z(t); S_{\mathbf{k}'}^z(0) \rangle \rangle = \langle S_{\mathbf{k}-\mathbf{k}'', -}^z \rangle G_{\mathbf{k}', \mathbf{k}'} \quad (2.5)$$

Hence

$$\langle S_{\mathbf{k}-\mathbf{k}'', -}^z \rangle = -S\sigma X_{\mathbf{k}-\mathbf{k}'', -}, \quad (2.6)$$

where

$$X_{\mathbf{k}-\mathbf{k}'', -} = N^{-1} \sum_{\alpha} \xi_{\alpha} e^{-i(\mathbf{k}-\mathbf{k}'') \cdot \tilde{r}_{\alpha}} \quad (2.7)$$

and

$$\langle S_{\alpha}^z \rangle = \xi_{\alpha} \langle S_{\alpha}^z \rangle = -\xi_{\alpha} S\sigma, \quad (2.8)$$

in which we assumed that  $\langle S_{\alpha}^z \rangle$  is *site independent*.  $\sigma$  depends both on  $x$ , the fraction of A-type atoms, and on the temperature  $T$ .  $\sigma$  will be calculated self-consistently in Sec. VI.

A Fourier transform of Eq. (2.4) with respect to  $t$  yields

$$\frac{\omega - \omega_H}{2S\sigma} G_{\mathbf{k}, \mathbf{k}'} = N^{-1} X_{\mathbf{k}-\mathbf{k}'} \\ - \sum_{\mathbf{k}''} (J_{\mathbf{k}'', -} - J_{\mathbf{k}', -\mathbf{k}''}) X_{\mathbf{k}-\mathbf{k}'', -} G_{\mathbf{k}', \mathbf{k}'}, \quad (2.9)$$

where  $\omega_H \equiv g\mu_B H$ . This equation can be written in a matrix form:

$$(\nu 1 - Y)G = N^{-1}X, \quad (2.10)$$

where  $X_{\mathbf{k}\mathbf{k}'} \equiv X_{\mathbf{k}-\mathbf{k}'}$ ,  $Y_{\mathbf{k}\mathbf{k}'} \equiv (J_{\mathbf{k}-\mathbf{k}'} - J_{\mathbf{k}', -\mathbf{k}})X_{\mathbf{k}\mathbf{k}'}$ , and  $\nu \equiv (\omega - \omega_H)/2S\sigma$ . Eq. (2.10) can be written

$$G = \mathcal{G}X, \quad (2.11)$$

where

$$\mathcal{G} = N(\nu 1 - Y).$$

$\mathcal{G}^{-1}$  can be broken up into two parts:

$$\mathcal{G}^{-1} = \mathcal{G}_0^{-1} - \Delta, \quad (2.12)$$

where  $\mathcal{G}_0^{-1}$  is the configuration average of  $\mathcal{G}^{-1}$ , i.e.,

$\mathcal{G}_0^{-1} = \bar{\mathcal{G}}^{-1} = N(\nu \mathbf{1} - \bar{Y})$  and  $\Delta \equiv N(Y - \bar{Y})$ . Note that  $\mathcal{G}_0^{-1}$  is diagonal, i.e.,  $(\mathcal{G}_0^{-1})_{\mathbf{k}\mathbf{k}'} = N[\nu - x(J_0 - J_{\mathbf{k}})] \delta_{\mathbf{k}\mathbf{k}'}$ .

It follows that  $\mathcal{G}$  obeys a Dyson equation:

$$\mathcal{G} = \mathcal{G}_0 + \mathcal{G}_0 \Delta \mathcal{G} \quad (2.13)$$

and hence  $G$  also obeys a Dyson equation:

$$G = \mathcal{G}_0 X + \mathcal{G}_0 \Delta \mathcal{G} X = \mathcal{G}_0 X + \mathcal{G}_0 \Delta G. \quad (2.14)$$

The configuration average of the Green's function  $\bar{G}$ , however, does not obey a Dyson-type equation. We are then faced with the problem of finding a self-consistent equation for  $G$ . This can be accomplished by iterating Eq. (2.14) once and decoupling  $(\Delta \mathcal{G}_0 \Delta G)_{\text{av}} \simeq (\Delta \mathcal{G}_0 \Delta)_{\text{av}} \bar{G}$ . In this approximation we obtain

$$\bar{G} = G_0 + G_0 \Sigma \bar{G}, \quad (2.15)$$

where  $G_0 = \mathcal{G}_0 [\bar{X} + (\Delta \mathcal{G}_0 X)_{\text{av}}]$  and  $G_0 \Sigma = \mathcal{G}_0 (\Delta \mathcal{G}_0 \Delta)_{\text{av}}$ .

To understand the spirit of the decoupling that was done, we note that the "exact" equation for  $\bar{G}$  is

$$\begin{aligned} \bar{G} = \mathcal{G}_0 [ & \bar{X} + (\Delta \mathcal{G}_0 X)_{\text{av}} + (\Delta \mathcal{G}_0 \Delta \mathcal{G}_0 X)_{\text{av}} \\ & + (\Delta \mathcal{G}_0 \Delta \mathcal{G}_0 \Delta \mathcal{G}_0 X)_{\text{av}} + \dots ]. \end{aligned} \quad (2.16)$$

Assuming that  $Y$  is distributed symmetrically around  $\bar{Y}$  we conclude that  $\Delta \equiv Y - \bar{Y}$  satisfies  $(\Delta^{2n+1})_{\text{av}} = 0$  for all  $n$ . Hence, in Eq. (2.16) it is quite natural to treat separately terms  $[(\Delta \mathcal{G}_0)^{2n} X]_{\text{av}}$  and  $[(\Delta \mathcal{G}_0)^{2n+1} X]_{\text{av}}$ . The former are decoupled according to  $[(\Delta \mathcal{G}_0)^{2n}]_{\text{av}} \bar{X}$  while the latter as  $[(\Delta \mathcal{G}_0)^{2n}]_{\text{av}} (\Delta \mathcal{G}_0 X)_{\text{av}}$ . We next adopt the approximation  $[(\Delta \mathcal{G}_0)^{2n}]_{\text{av}} \simeq [(\Delta \mathcal{G}_0)^2]_{\text{av}}^n$ . Inserting all these into Eq. (2.16) we obtain

$$\begin{aligned} \bar{G} &= \mathcal{G}_0 [\bar{X} + (\Delta \mathcal{G}_0 X)_{\text{av}} \{1 - [(\Delta \mathcal{G}_0)^2]_{\text{av}}\}^{-1} \\ &= G_0 (1 - G_0 \Sigma), \end{aligned} \quad (2.17)$$

which is exactly Eq. (2.15).

The present approximation for  $\bar{G}$  is quadratic in  $\Delta$ . However, as will be shown later, only a subgroup of these quadratic terms is included in this approximation; hence, it will be referred to as the "low quadratic approximation" (LQA).

The averages may be all shown to be diagonal.

$$\begin{aligned} (\zeta_{\alpha_1} \zeta_{\alpha_2} \dots \zeta_{\alpha_n})_{\text{av}} &= P_n(x) \delta_{\{\alpha\}} + P_{n-1}(x) P_1(x) \sum_{i=1}^n \delta_{\{\alpha\}_i} + P_{n-2}(x) P_1^2(x) \sum_{i,j} \delta_{\{\alpha\}_{ij}} \\ &+ P_{n-2}(x) P_2(x) \sum_{i,j} \delta_{\{\alpha\}_{ij}} \delta_{\alpha_i \alpha_j'} + \dots + P_1^n(x), \end{aligned} \quad (3.1)$$

where  $\delta_{\{\alpha\}}(\delta_{\{\alpha\}_i}, \delta_{\{\alpha\}_{ij}}, \text{etc.})$  assumes the value unity, provided all  $\alpha_k$ 's (all  $\alpha_k$ 's but for  $\alpha_i$ , all  $\alpha_k$ 's but for  $\alpha_i$  and  $\alpha_j$ , etc.) are equal, and zero otherwise.

Introducing the reduced frequency  $\Omega = \nu/x$  [where  $\nu$  was defined in Eq. (2.10)], the averages are expressed by

$$\bar{X}_{\mathbf{k},\mathbf{k}'} = x \delta_{\mathbf{k},\mathbf{k}'}, \quad (2.18a)$$

$$\begin{aligned} [(\Delta \mathcal{G}_0 X)_{\text{av}}]_{\mathbf{k},\mathbf{k}'} &= -(1-x) P(\mathbf{k}, \Omega) \delta_{\mathbf{k},\mathbf{k}'} \\ &\equiv -(1-x) N^{-1} \sum_{\mathbf{q}} \frac{J_{\mathbf{k}-\mathbf{q}} - J_{\mathbf{q}}}{J_0 - J_{\mathbf{q}} - \Omega}, \end{aligned} \quad (2.18b)$$

$$\begin{aligned} [(\Delta \mathcal{G}_0 \Delta)_{\text{av}}]_{\mathbf{k},\mathbf{k}'} &= -N(1-x) Q(\mathbf{k}, \Omega) \delta_{\mathbf{k},\mathbf{k}'} \\ &\equiv -(1-x) \\ &\times \sum_{\mathbf{q}} \frac{(J_{\mathbf{k}-\mathbf{q}} - J_{\mathbf{q}})(J_{\mathbf{k}-\mathbf{q}} - J_{\mathbf{q}})}{J_0 - J_{\mathbf{q}} - \Omega}. \end{aligned} \quad (2.18c)$$

Hence, we finally obtain for  $\bar{G}$

$$\bar{G}_{\mathbf{k},\mathbf{k}'} = N^{-1} \frac{1 - [(1-x)/x] P(\mathbf{k}, \Omega)}{\Omega - (J_0 - J_{\mathbf{k}}) + [(1-x)/x] Q(\mathbf{k}, \Omega)} \delta_{\mathbf{k},\mathbf{k}'}. \quad (2.19)$$

### III. DIAGRAMMATIC REPRESENTATION AND THE "HIGH QUADRATIC APPROXIMATION" (HQA)

The Green's function and the averaging process of Sec. II may be represented diagrammatically as follows: we start by representing Eq. (2.16) for the unaveraged Green's function by the diagram in Fig. 1. Here a straight line with wave number  $\mathbf{k}_i$  represents  $\mathcal{G}_{0\mathbf{k}_i}$ , and a point associated with  $M$ , flanked by lines of wave numbers  $\mathbf{k}_i$  and  $\mathbf{k}_j$ , represents the matrix element (in  $\mathbf{k}$  space)  $M_{\mathbf{k}_i\mathbf{k}_j}$  of a random matrix  $M$ . Also the summation convention over internal lines is implicitly assumed.

Each variable  $M_{\mathbf{k}_i\mathbf{k}_j}$  in this problem contains a sum over sites of the random occupation numbers  $\zeta_{\alpha}$  at a site  $\alpha$ , namely,

$$N^{-1} \sum_{\alpha} \zeta_{\alpha} e^{i(\mathbf{k}_i - \mathbf{k}_j) \cdot \mathbf{r}_{\alpha}} m_{\mathbf{k}_i\mathbf{k}_j}$$

Thus, on averaging an  $n$ -point diagram, one needs to express the average  $(\zeta_{\alpha_1} \dots \zeta_{\alpha_n})_{\text{av}}$ . This can be shown to be

$P_n(x)$  are the polynomials given by<sup>17</sup>

$$P_n(x) = \left[ \left( \frac{\partial}{\partial y} \right)^n \ln(1 - x + x e^y) \right]_{y=0}, \quad (3.2)$$

$$G_{\vec{k}, \vec{k}} = \frac{\vec{k}' \vec{k}}{x} + \frac{\vec{k}' \vec{k}_1 \vec{k}}{\Delta x} + \frac{\vec{k}' \vec{k}_1 \vec{k}_2 \vec{k}}{\Delta \Delta x} + \dots$$

FIG. 1. Diagrammatic representation of Eq. (2.16). A straight line with wave number  $\vec{k}_1$  represents  $g_{0\vec{k}_1}$ . A point associated with  $M_i$  flanked by lines of wave numbers  $k_i$  and  $k_j$ , represents the matrix element  $M_{k_i k_j}$ .

where the lowest-order polynomials are

$$P_1(x) = x, P_2(x) = x(1-x), P_3(x) = x(1-x)(1-2x).$$

Equation (3.1) may be represented by the diagram in Fig. 2. Here, to any site  $\alpha_i$ , a line with wave number  $\vec{k}_i$  enters and  $\vec{k}_{i+1}$  leaves. Sites  $\alpha_i, \alpha_j$ , etc., that are equal under the  $\delta$ -function constraint are connected by dashed lines. In Fig. 2, all topologically different diagrams, and the polynomials associated with them, are included. It is easily seen that wave numbers of internal lines are free variables and have to be summed over, while disconnected sites lead to a  $\delta$ -function conservation of the incoming and outgoing wave numbers. Thus, if a disconnected point is associated with a matrix  $M$  it clearly gives  $\bar{M}$ . In our particular case if  $M = \Delta$ , this diagram vanishes (since by definition  $\bar{\Delta} = 0$ ).

Returning now to Eq. (2.16) the simplest non-trivial approximation to the averaged Green's function may be obtained by retaining only the diagrams in which *pairs of nearest-neighbor* points are connected. This is shown in Fig. 3. Calculating the diagrams according to the rules mentioned above and shown in Fig. 4, we find

$$\bar{G}_{\vec{k}, \vec{k}} = \left( X + P_2(x) \sum_{\vec{q}} g_{0\vec{q}} (J_{\vec{k}-\vec{q}} - J_{\vec{q}}) \right) \delta_{\vec{k}, \vec{k}} \times \left( 1 - P_2(x) \sum_{\vec{q}} g_{0\vec{q}} (J_{\vec{k}-\vec{q}} - J_{\vec{q}})(J_{\vec{k}-\vec{q}} - J_{\vec{q}}) \right)^{-1}, \quad (3.3)$$

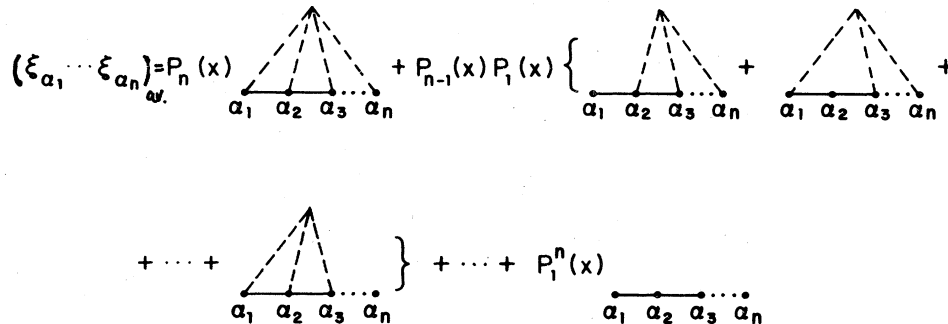


FIG. 2. Diagrammatic representation of the configurational average of  $\xi_{\alpha_1} \dots \xi_{\alpha_n}$ . Here the dots represent sites  $\alpha_n$ . Connected sites are identical.

which is just the LQA result of Eq. (2.19). We can improve upon the LQA, still within the quadratic approximation, if we retain all the diagrams with *connected pairs* of points (not only nearest-neighbor points), provided that the dashed lines do not intersect. These diagrams are shown and summed up in Figs. 5 and 6.

It becomes clear from the last line in Fig. 5 that  $\bar{G}_{\vec{k}, \vec{k}}$  has an expression similar to Eq. (2.19) but with  $P$  and  $Q$  replaced by  $P_H$  and  $Q_H$  which satisfy the integral equations

$$Q_H = \sum_{\vec{q}} \frac{(J_{\vec{k}-\vec{q}} - J_{\vec{q}})(J_{\vec{k}-\vec{q}} - J_{\vec{q}})}{\Omega - (J_0 - J_{\vec{q}}) + [(1-x)/x] Q_H(\vec{q}, \Omega)} \quad (3.4)$$

and

$$P_H = \sum_{\vec{q}} \frac{J_{\vec{k}-\vec{q}} - J_{\vec{q}}}{\Omega - (J_0 - J_{\vec{q}}) + [(1-x)/x] Q_H(\vec{q}, \Omega)}. \quad (3.5)$$

We call this approximation the "high quadratic approximation" (HQA).

In the next Secs. IV and V it will be shown that in calculating static properties, such as critical temperature, critical concentration, etc., the LQA provides rather good agreement with experimental or exact numerical results; for dynamic properties, such as the response function, which depend sensitively on the imaginary part of  $\bar{G}$ , we have to use the HQA to get reasonable agreement with exact numerical calculations.

At the high-concentration limit ( $x \sim 1$ ) it follows from Eqs. (3.4) and (3.5) that the LQA and the HQA coincide; they both deviate, however, from the exact result. To lowest order in  $1-x$ , one has to sum all the diagrams shown in Fig. 7, which represent repeated scattering from the same site [since  $P_i(x) \propto (1-x)$  for  $n > 1$ ]. An estimate of the discrepancy between our LQA result and the exact expansion<sup>24</sup> is discussed in Sec. V.

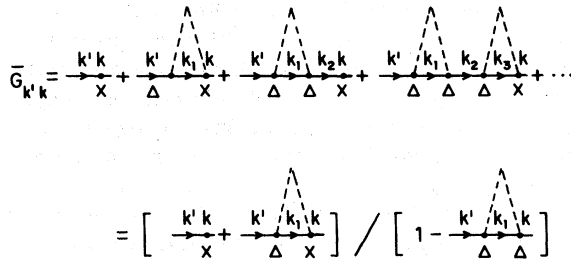


FIG. 3. The sum of diagrams for  $\bar{G}$  which are taken into account in the low quadratic approximation (LQA).

#### IV. FERROMAGNETIC CRITICAL TEMPERATURE AND CONCENTRATION

The ferromagnetic critical temperature  $T_c(x)$  has been shown to be related to the configurationally averaged Green's function by<sup>25,26</sup>

$$\beta_c(x) = -\frac{2}{x} \sum_{\vec{k}} \text{Re} G_{\vec{k}\vec{k}}(\Omega=0) \Big|_{\omega_H=0}, \quad (4.1)$$

where  $\beta_c = 1/(k_B T_c)$ . Using the LQA result, Eq. (2.19) becomes

$$\beta_c(x) = \frac{2}{x} N^{-1} \sum_{\vec{k}} \frac{1 - [(1-x)/x] P(\vec{k}, 0)}{J_0 - J_{\vec{k}} - [(1-x)/x] Q(\vec{k}, 0)}, \quad (4.2)$$

where in Eq. (4.2) we used the fact that both  $P$  and  $Q$  are real at  $\Omega=0$  (cf. Appendix).

We have calculated  $T_c(x)$  for the three cubic lattices, taking into account first- and second-neighbors interactions. This was repeated for several values of  $\eta = J_2/J_1$ , the ratio of second- to first-neighbor interactions. For this purpose  $P(\vec{k}, 0)$  and  $Q(\vec{k}, 0)$  were expressed as a sum of products like  $f(\vec{k})C(\eta)$ , where  $f(\vec{k})$  is an explicit function of  $\vec{k}$  and  $C(\eta)$  depends on lattice structure and calculated numerically (cf. Appendix). Results for  $T_c(x)$  are shown in Fig. 8. It can be seen that all the  $T_c(x)$  graphs are fairly linear functions of  $x$ ,

$$\begin{aligned} \frac{k'k}{x} &= x \delta_{k'k} \\ \frac{k'k_1k}{\Delta} &= x(1-x) \sum_{\vec{k}_1} g_{\vec{k}_1} (J_{k'-k_1} - J_{k_1}) \delta_{k'k} \\ \frac{k'k_1k_2k}{\Delta^2} &= x(1-x) \sum_{\vec{k}_1} g_{\vec{k}_1} (J_{k'-k_1} - J_{k_1}) (J_{k_1-k_2} - J_{k_2}) \delta_{k'k} \end{aligned}$$

FIG. 4. Glossary of diagrammatic symbols used in Fig. 3.

except in the vicinity of  $x_c$ , where they all exhibit a certain curvature. This kind of behavior was predicted earlier<sup>1-4</sup> and was found experimentally.<sup>27-29</sup>

In Fig. 9 the reduced critical temperature  $T_c(x)/T_c(1)$  is plotted against the reduced concentration  $\xi = (x - x_c)/(1 - x_c)$ . It can be seen that for  $\eta \geq 0$  (for all three cubic lattices) the plots fall on a single universal curve. The  $\eta < 0$  curves, however, deviate quite considerably from this universal curve.

It can also be seen that for each  $\eta$  there exists a critical concentration  $x_c$  for which

$$T_c(x_c) = 0 \quad \beta_c(x_c) \rightarrow \infty. \quad (4.3)$$

From Eq. (4.2),  $T_c$  may be easily shown to behave like  $|x - x_c|^{1/2}$  near  $x_c$ .

Values of  $x_c(\eta)$  are presented in Table I for all three cubic lattices. For the cases of  $\eta=0$  and  $\eta=1$ , these can be compared with the corresponding site-percolation concentration<sup>30</sup>  $p_c$  (either for nn steps in the case  $\eta=0$ , or both nn and second-neighbors steps in the case of  $\eta=1$ ). We have also calculated  $x_c$  including third-neighbors interactions. The special case  $J_1 = J_2 = J_3$  is also tabulated and shown to agree with the corresponding percolation concentration.

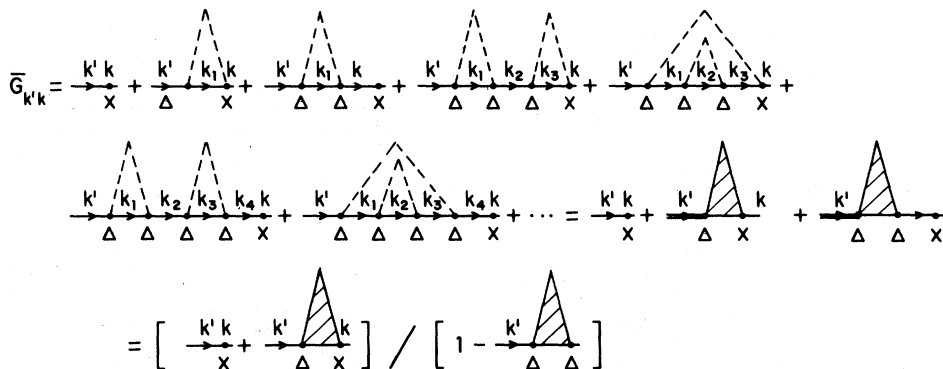


FIG. 5. Same as in Fig. 3 but in the high quadratic approximation (HQA).

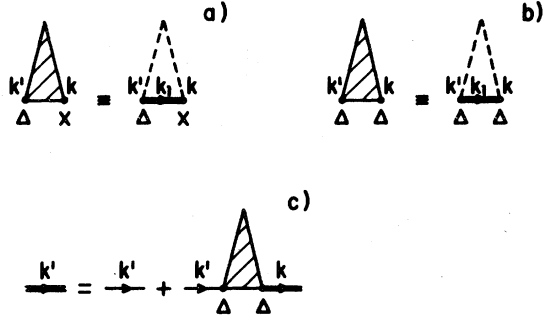


FIG. 6. Glossary of diagrammatic symbols used in Fig. 5.

### V. EXCITATION AND DENSITY OF STATES FOR A SC CRYSTAL FOR NN INTERACTIONS

The excitations of the system can be studied from the spectral weight function,  $\rho_{\vec{k}}(\Omega) = -\pi^{-1} \text{Im} \bar{G}_{\vec{k}}(\Omega)$ . As usual, one defines dispersion relation  $\Omega(\vec{k})$  from the condition that the response function  $\rho_{\vec{k}}(\Omega)$  is maximal at  $\Omega(\vec{k})$ .

For small  $k$ , the maxima of  $\rho_{\vec{k}}(\Omega)$  are obtained at  $\Omega \ll 2J_1 Z_1$ , where  $z_1$  is the number of nearest neighbors (in a perfect crystal  $0 < \Omega < 2J_1 Z_1$ ). Since at low  $\Omega$ ,  $\text{Im} Q(\vec{k}, \Omega)$  is very small, these maxima are rather sharp and thus correspond to "good," long-lived excitations. Here both the LQA and the HQA give similar results. We shall thus for simplicity discuss the  $k \rightarrow 0$  limit in the LQA. At large  $k$ , however, the LQA underestimates  $\text{Im} Q(\vec{k}, \Omega)$ , i.e., the width of the maxima of  $\rho_{\vec{k}}(\Omega)$ . Moreover, when the maxima are obtained at  $\Omega > 2J_1 Z_1$ ,  $\text{Im} Q(\vec{k}, \Omega)$  in the LQA vanishes abruptly and anomalously sharp maxima ( $\delta$  function) are obtained for  $\rho$ . It is thus imperative to use the HQA for large  $k$ . The dispersion relation  $\Omega(\vec{k})$  in the small  $k$  region are found from the zeros of the real part of  $\bar{G}_{\vec{k}}^{-1}$  [Eq. (2.19)], i.e.,

$$\Omega(\vec{k}) - (J_0 - J_{\vec{k}}) + [(1-x)/x] Q(\vec{k}, \Omega(\vec{k})) = 0. \quad (5.1)$$

This is an implicit equation in  $\Omega$  which has to be solved numerically. For  $k \rightarrow 0$ , however,  $Q(\vec{k}, \Omega)$

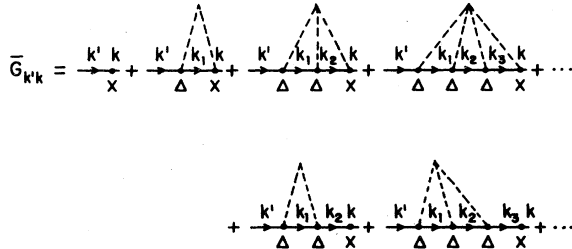


FIG. 7. The series of all diagrams for  $\bar{G}$  to order  $(1-x)$ .

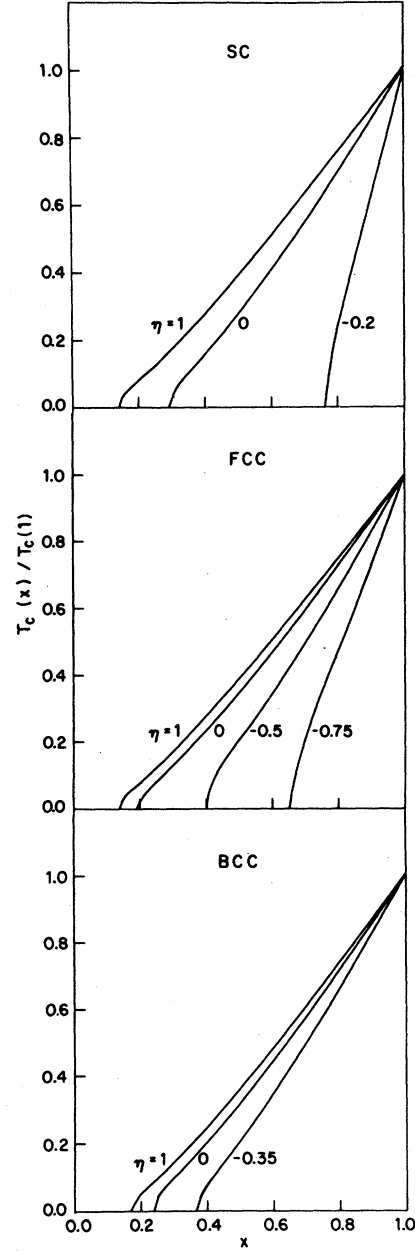


FIG. 8. Ferromagnetic reduced critical temperature  $T_c(x)/T_c(1)$  vs concentration  $x$  for different values of  $\eta$ —the ratio between second- and first-nn interactions.

$\sim Q_0 k^2$  and  $J_0 - J_{\vec{k}} \sim L k^2$ , and Eq. (5.1) yields

$$\Omega(\vec{k}) = \{L - [(1-x)/x] Q_0\} k^2 = \phi(x) k^2. \quad (5.2)$$

$L$  and  $Q_0$  are structure-dependent constants:  $L = \sum J_i l_i a^2$  where  $a$  is the lattice constant and the  $l_i$ 's are given in Table II.  $Q_0$  is given by  $Q_0 = N^{-1} \sum_{\vec{q}} |\nabla_{\vec{q}} J_{\vec{q}} \cdot \vec{k}|^2 / (J_0 - J_{\vec{q}})$  and can be calculated from the explicit expression for  $Q$ , Eq. (A5).

A similar result was obtained by Murray<sup>14</sup> and

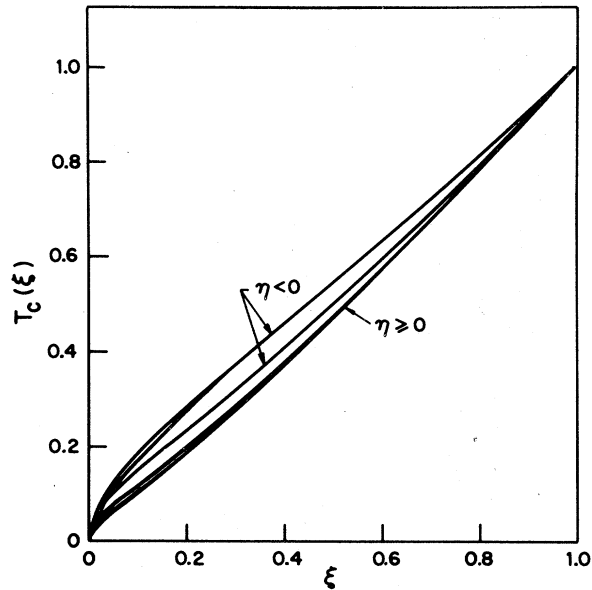


FIG. 9.  $T_c(x)/T_c(1)$  from Fig. 8 plotted vs the reduced concentration  $\xi = x - x_c(\eta)/(1 - x_c(\eta))$ .

TABLE I. Critical concentration  $x_c$  vs  $\eta \equiv J_2/J_1$ —the ratio between second nn and nn interactions—for the three cubic lattices.

Lattice	$\eta$	$x_c(\eta)$	$p_c$ from Ref. 29
sc	-0.2	0.763	
	-0.1	0.444	
	0	0.296	0.307
	0.1	0.223	
	0.25	0.174	
	0.50	0.147	
	1.00	0.141	0.137
	$J_1 = J_2 = J_3$	0.102	0.097
bcc	-0.5	0.479	
	-0.2	0.297	
	-0.1	0.264	
	0	0.240	0.243
	0.25	0.202	
	0.5	0.185	
	1.00	0.176	0.175
	$J_1 = J_2 = J_3$	0.101	0.095
fcc	-0.95	0.936	
	-0.75	0.656	
	-0.50	0.403	
	0	0.197	0.195
	0.25	0.163	
	0.5	0.147	
	1	0.140	0.136
	$J_1 = J_2 = J_3$	0.066	0.061

TABLE II. Several topological properties of the cubic lattices.

Lattice	$i$ Shell number	$z_i$ Number of atoms in the $i$ th shell	$l_i$	$N_{11}(i)$ Covering factors for the $i$ th shell (see Appendix)	$N_{12}(i)$	$N_{22}(i)$
sc	1	6	1	0	4	0
	2	12	4	2	0	4
	3	8	4	0	3	0
	4	6	4	1	0	4
	5	24	20	0	1	0
	6	24	24	0	0	2
	7 <sup>a</sup>	...	...	...	...	...
	8	12	16	0	0	1
fcc	1	12	1	4	2	0
	2	6	1	4	0	0
	3	24	6	2	1	0
	4	12	4	1	0	2
	5	24	10	0	1	0
	6	8	4	0	0	0
	7	48	28	0	0	0
	8	6	4	0	0	1
bcc	1	8	1	0	3	0
	2	6	1	4	0	0
	3	12	4	2	0	2
	4	24	11	0	1	0
	5	8	4	1	0	0
	6	6	4	0	0	1
	7	24	19	0	0	0
	8	24	20	0	0	0

<sup>a</sup> For an sc lattice, the  $i$ th-shell distance  $a_i$  satisfies  $a_i = \sqrt{i}a$  for all  $i$  in this table except  $i=7$ . In this sense no seventh shell exists.

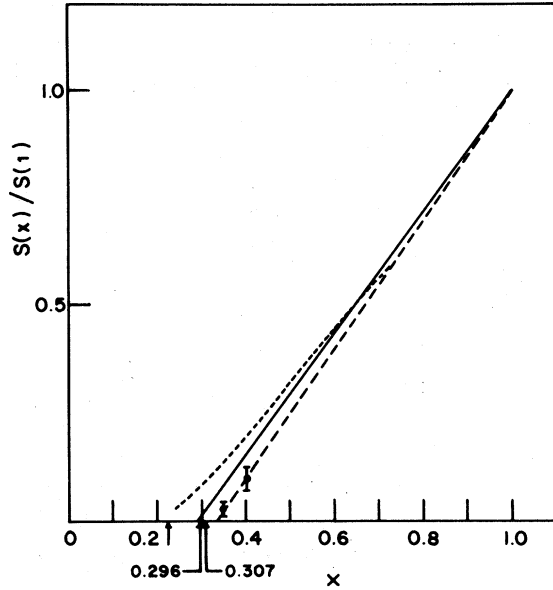


FIG. 10. Spin-wave stiffness as function of concentration  $x$ . Long-dashed line—Monte Carlo calculations of Ref. 31. Short-dashed line—CPA results of Ref. 22. Full—results of this paper. 0.307 and 0.296 indicate values of  $x_c$  of Ref. 31 and this paper, respectively.

used to calculate the critical concentration by the condition that  $\phi(x)$  vanishes at  $x_c$ . It follows that for  $x < x_c$ , where  $\phi(x) < 0$ , no physical excitations exist.

The spin-wave stiffness  $S(x)$  is proportional to  $x\phi(x)$ . At zero temperature the ratio  $S(x)/S(1)$  is a straight line which cuts the  $x$  axis at  $x = x_c$ . In Fig. 10,  $S(x)/S(1)$  is shown and compared to Monte Carlo calculations by Kirkpatrick<sup>31</sup> and to CPA results by Theumann *et al.*<sup>22</sup>

It is apparent that near  $x_c$  our  $S(x)/S(1)$  agrees quite well with "exact" result.<sup>31</sup> At  $x \sim 1$ , however, our result deviates slightly from the CPA results.<sup>20,21</sup> These coincide in the  $x \sim 1$  region with the "exact" calculated  $S(x)/S(1)$  of Izyumov,<sup>24</sup> namely,

$$S(x)/S(1) = 1 - \Lambda_{IZ}(1-x) + O(1-x)^2, \quad (5.3)$$

where  $\Lambda_{IZ}$  is a numerical factor equal to 1.52. Our  $S(x)/S(1)$ , on the other hand, can be shown from Eq. (5.2) to be equal to  $1 - \Lambda(1-x)$  with  $\Lambda = 1/(1-x_c) \approx 1.42$ .

For large  $k$ ,  $\rho_{\vec{k}}(\omega)$  is calculated using the HQA result for  $\mathcal{G}$ , with  $P_H$  and  $Q_H$  given by Eqs. (3.4) and (3.5). One finds that the maxima of  $\rho_{\vec{k}}(\omega = 2S\omega)$  shift continuously to lower energies (for fixed  $\vec{k}$ ) as  $x$  is decreased. In Figs. 11–14 the present results for  $\rho_{\vec{k}}(\omega)$  are compared, for some values of  $x$  and  $k$ , with those of Theumann and Tahir-Kheli,<sup>22</sup> Harris *et al.*<sup>20</sup> (CPA calculations), and Nickel<sup>23</sup>

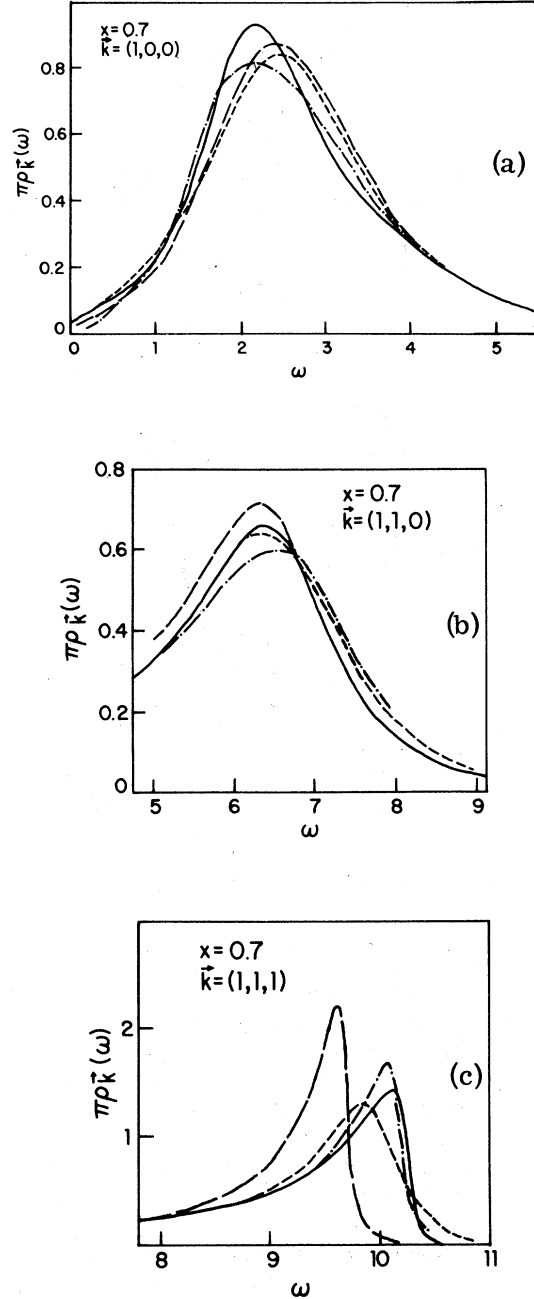


FIG. 11. Response function of  $\rho(\vec{k}, \omega)$  plotted vs  $\omega$  for concentration  $x$  and wave vector  $\vec{k}$  (in units of  $\pi/a$ ) indicated on the figure. Full line—this work; dash-dot—Ref. 22; long dashed—Ref. 20; short dashed—Ref. 23 ("exact" result).

(Padé-moment calculations). For  $k$  large enough, and  $x < 0.7$ , an additional low-energy peak in  $\rho_{\vec{k}}(\omega)$  appears. As  $x$  is decreased, the low-energy peak becomes more pronounced, as much as half the height of the central peak. Of the references mentioned above only Nickel's has these low-energy



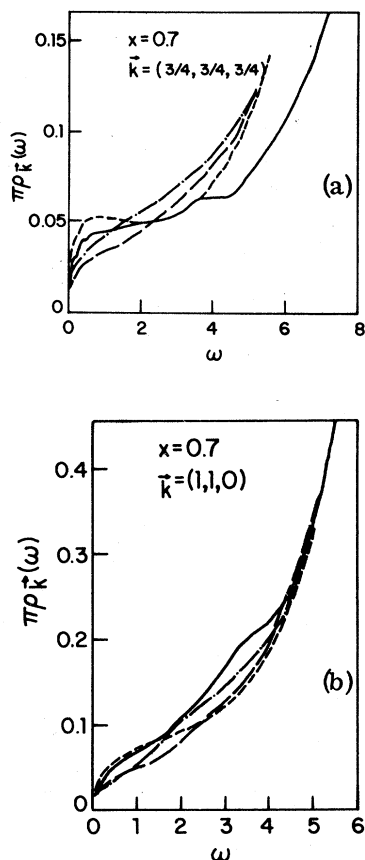


FIG. 12. Caption same as in Fig. 11. A blow up of the low- $\omega$  region.

peaks; however, their height is somewhat lower and their location at lower energy than ours.

The central peak locations of  $\rho_{\vec{k}}(\Omega)$ ,  $\text{Re}\Omega(\vec{k})$ , and width at half-maximum,  $\text{Im}\rho(\vec{k})$  are compared in Fig. 15 to CPA results by Harris *et al.*<sup>20</sup> (which are in fair agreement with  $\text{Re}\Omega(\vec{k})$  Padé-moment results by Nickel.<sup>23</sup>

The two-peak structure of  $\rho_{\vec{k}}(\Omega)$  that was found for  $x < 0.7$  and for large enough  $k$  is also apparent in the corresponding dispersion relation  $\omega(\vec{k})$  which we have plotted for  $\vec{k}$  in the (1,1,1) direction, in Fig. 16. At large  $x$  there is a single branch of  $\omega(\vec{k})$  for all  $k$ . At lower  $x$  ( $< 0.70$ ), however,  $\omega(\vec{k})$  splits into two branches for  $k$  greater than some  $k_0(x)$ . This kind of dispersion relation appears also in Elliot *et al.*<sup>19</sup>

It was suggested<sup>19,20</sup> that the additional lower branch, which begins to appear at large  $k$  as  $x$  is lowered, may be associated with excitation within finite isolated clusters. These have a finite probability of existing for concentrations not too far above (or below) the percolation concentration  $p_c$ .

The density of states of the spin-wave excitations is given by

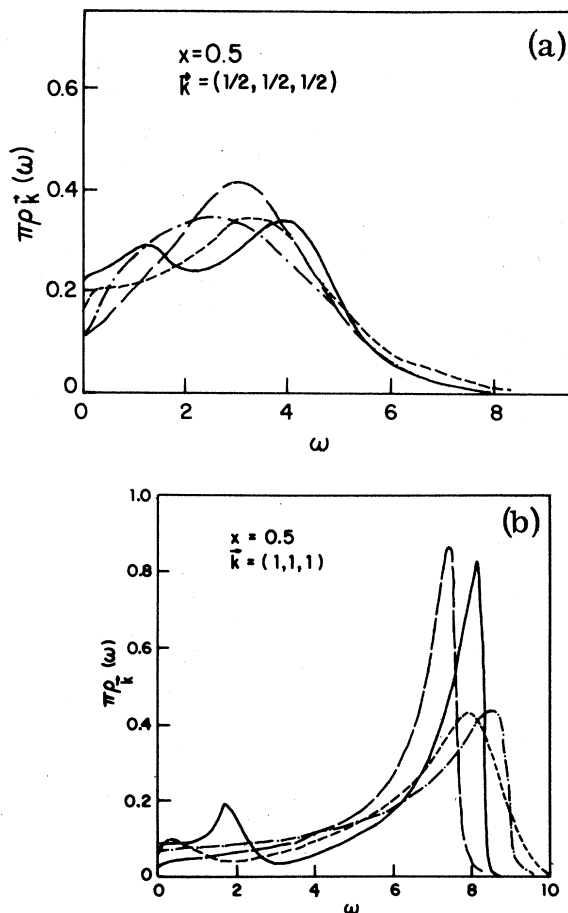


FIG. 13. Caption same as in Fig. 11.

$$D(\Omega) = -\frac{1}{\pi} \sum_{\vec{k}} \text{Im}(G_{\vec{k}\vec{k}})_{av}(\Omega) \quad (5.4)$$

and can be shown to be normalized to unity. Accordingly, we have for the density of states in terms of  $\omega$  ( $= 2S\alpha x\Omega$ )

$$\int_{-\infty}^{\infty} d\omega \mathcal{D}(\omega) = 2S\alpha x. \quad (5.5)$$

$\mathcal{D}(\omega)$  is shown in Fig. 17 for several values of  $x$ . It is apparent that for medium  $x$  (below 0.7) the full density of states is composed of two separate contributions: a "finite cluster" contribution which tends to peak sharply at low energies, and "bulk" contribution which extends to high energies. This is compared in Fig. 18 with Theumann and Tahir-Kheli<sup>22</sup> and Harris *et al.*<sup>20</sup> which do not exhibit the two-peak structure.

It is quite interesting to note that a somewhat similar density of states was obtained by Montgomery *et al.*<sup>24</sup> for the problem of a pure ferromagnet with random exchange interactions. For large degree of disorder (i.e., for wide distribution of the

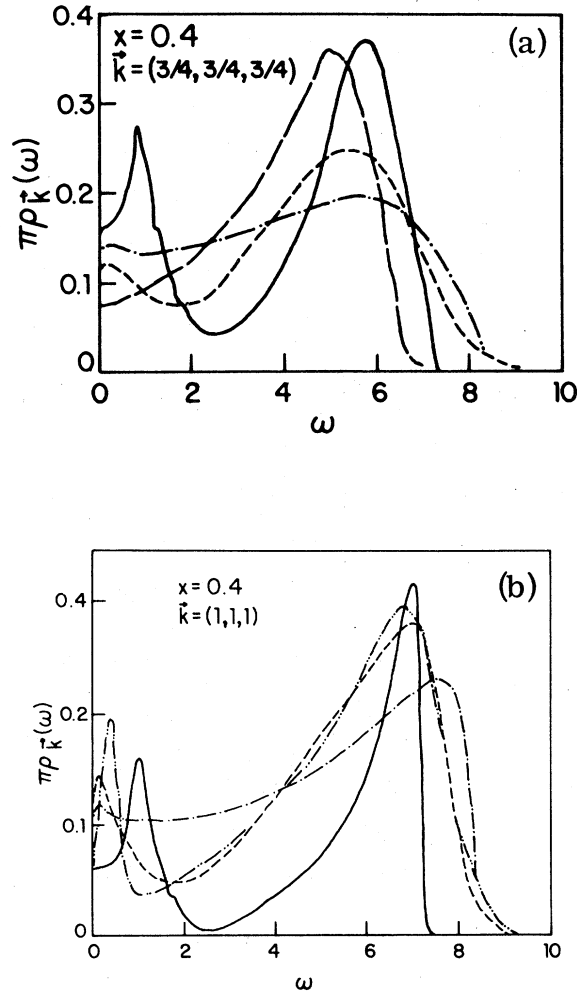


FIG. 14. Caption same as in Fig. 11. In addition the dash double dot represents Nickel's calculation with only eight exact moments.

$J$ 's) they also found a double peak in the density of states.

We now return to the excitations below the critical concentration  $x_c$ . As is apparent from Fig. 14, there exists, for all  $x < x_c$ , a cutoff wave vector  $k_c(x)$  such that for  $k < k_c(x)$ ,  $\omega < 0$ . Hence, no physical excitation exists. The inverse of  $k_c(x)$ , more precisely  $\pi k_c^{-1}$ , may be interpreted as the linear dimension of the largest cluster that the system can sustain. Clearly for  $x < x_c$ , no bulk ferromagnetism exists ( $\sigma = 0$ ), and hence no long-wavelength excitations. However, within a finite cluster  $[l_0 \sim \pi/k_c(x)]$ , there may still be a solution with  $\sigma \neq 0$  (where  $\sigma$  refers to the cluster magnetization) which can be obtained from Eqs. (6.4) and (6.5), provided that the sum over  $k$  excludes the region  $k < k_c(x)$ . Following this reasoning, we have calculated for some values of  $x < x_c$ , the number of

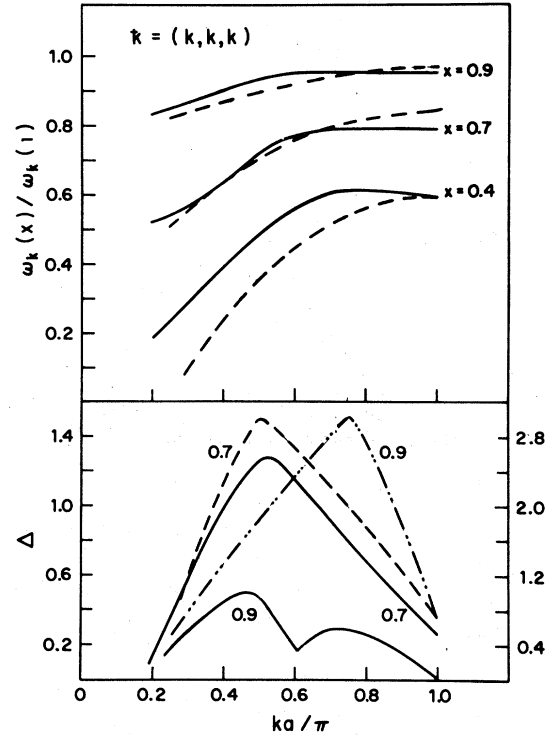


FIG. 15. Top section—central peak location of  $\rho_{\vec{k}}(\omega, x)$ , normalized to those of  $\rho_{\vec{k}}(\omega, 1)$ . Full line—CPA results of Ref. 31; dashed line—this paper. Bottom section—width of half-maximum  $\Delta$  of the central peak, in units of  $J$ . Full line—Ref. 20; dashed line—this paper. The ordinate on the left refers to  $x = 0.9$ , the one on the right to  $x = 0.7$ .

the magnetic atoms  $\bar{n}$  in the largest cluster. These are presented in Fig. 19 and compared with values deduced from calculations of the *average* cluster size of type-A atoms in a substitutional A-B alloy,<sup>10,11</sup> The discrepancy between the two methods, for  $x$  close to  $x_c$ , seems to originate from the fact that their  $\bar{n}$  behaves as  $(x_c - x)^{-1.6875}$  (with  $x_c \sim 0.28$ ), while in our calculation  $\bar{n} = (x_c - x)^{-3/2}$  (with  $x_c = 0.296$ ). The exponent  $-3/2$  is obtained as follows: close to  $x_c$ ,  $\omega_{\vec{k}}$  satisfies the equation

$$\omega_{\vec{k}} \sim \phi(x)k^2 + \psi(x)k^4, \quad (5.6)$$

where  $\phi(x) \sim -|x_c - x|$  and where  $\psi(x)$  is regular near  $x_c$ . Since  $k_c$  is obtained by the equation

$$\omega(k_c) = 0, \quad (5.7)$$

it follows from Eq. (5.5) that  $k_c \sim |x_c - x|^{1/2}$ . Since  $\bar{n} \sim l_0^3 \sim k_c^{-3}$ , we finally obtain  $\bar{n} \sim |x_c - x|^{-3/2}$ . More recent calculations<sup>32</sup> of this exponent fall in the region 1.66–1.80.

## VI. MAGNETIZATION AND HEAT CAPACITY

In order to derive an equation for the relative magnetization we recall the identity

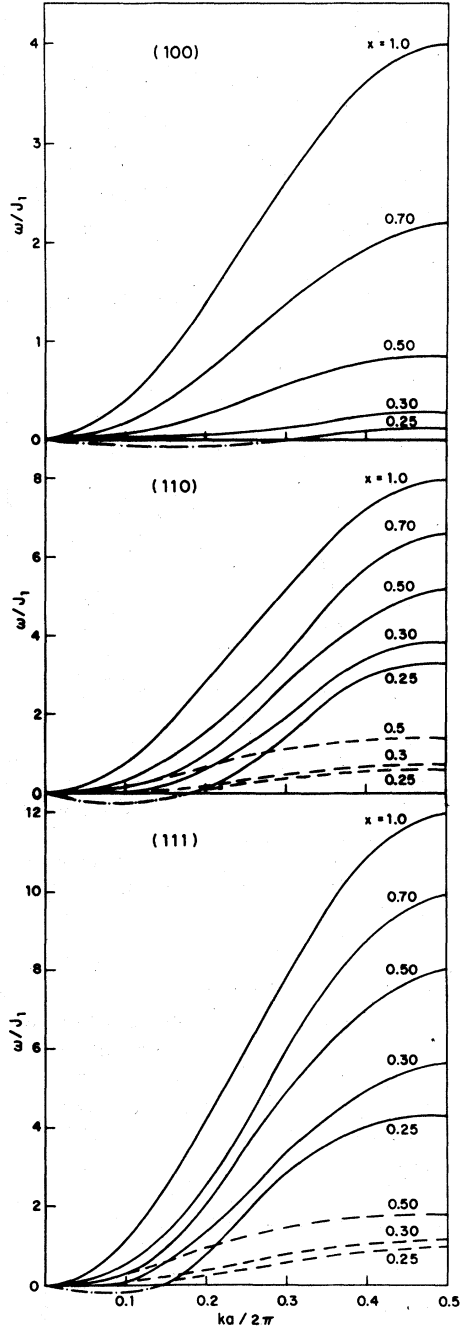


FIG. 16. Dispersion relation  $\omega(k)$  for different concentrations  $x$ . The dashed lines are secondary branch arising from local excitations. This is done for the three principal directions  $(1,0,0)$ ,  $(1,1,0)$ , and  $(1,1,1)$  for sc lattice.

$$S^+S^- + S^{z^2} - S^z = S(S+1). \quad (6.1)$$

Applying this identity to  $\vec{S}_\alpha \equiv \zeta_\alpha \vec{S}_\alpha$  and averaging both over the thermal ensemble and over random configurations

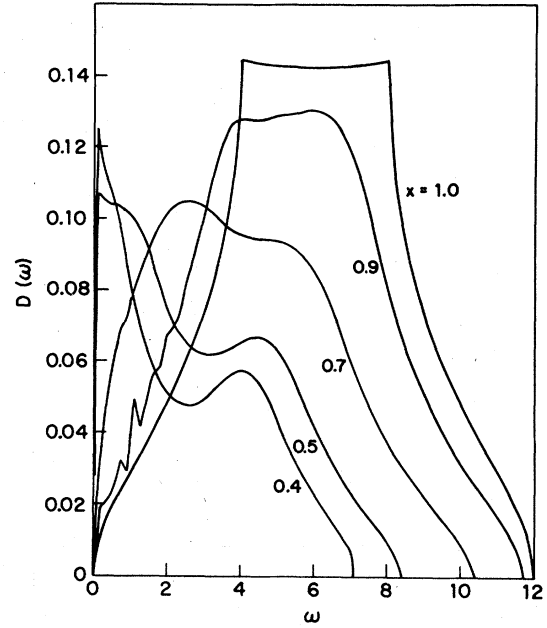


FIG. 17. Density of states for spin-wave excitation for several concentrations  $x$ . For sc lattice.

$$\langle (\vec{S}_\alpha^+ \vec{S}_\alpha^-)_{av} \rangle + \langle (\vec{S}_\alpha^z)^2_{av} \rangle - \langle \vec{S}_\alpha^z_{av} \rangle = xS(S+1). \quad (6.2)$$

As was stated earlier,  $\langle \vec{S}_\alpha^z \rangle = x\sigma S$ . Hence

$$\langle (\vec{S}_\alpha^+ \vec{S}_\alpha^-)_{av} \rangle + \langle (\vec{S}_\alpha^z)^2_{av} \rangle - \langle \vec{S}_\alpha^z_{av} \rangle = xS(S+1). \quad (6.3)$$

$\langle S_\alpha^z \rangle$  varies between  $S^2$  and  $S(S+1)/3$  as the tem-

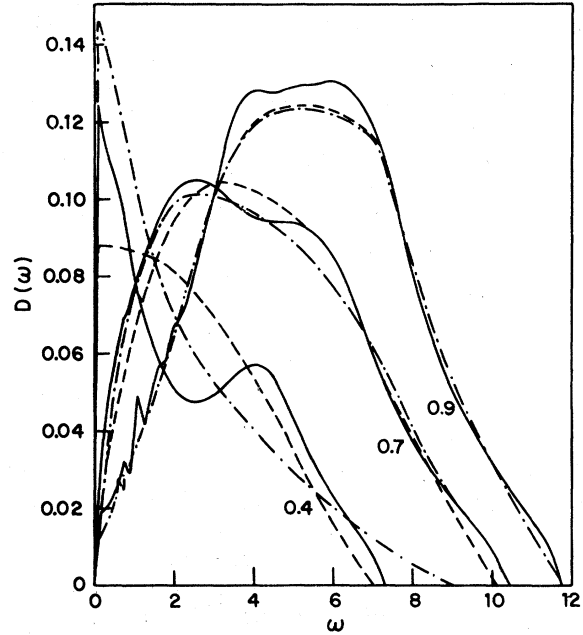


FIG. 18. Density of states (full line) compared for three different concentrations with parallel results of Ref. 22 (dash-dot) and of Ref. 20 (dashed).

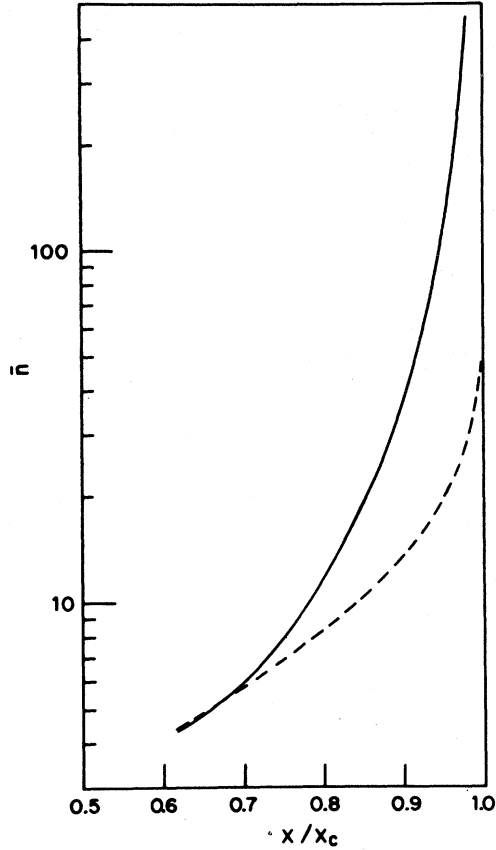


FIG. 19. The number of atoms  $\bar{n}$  in the *largest* magnetic cluster plotted vs the concentration  $x$  for the region  $x < x_c$ . The dashed curve represents values deduced from Ref. 10 for the *average* number of atoms in a magnetic cluster. For sc lattice.

perature is raised from zero to  $T_c$  and may be calculated from the equation

$$\langle S^z \rangle - \langle S^z \rangle^2 = (g\mu_B H)^{-1} \partial \langle S^z \rangle / \partial H.$$

For an  $S = \frac{1}{2}$  system, however,  $\langle S_\alpha^z \rangle = \frac{1}{3} S(S+1) = S^2$  identically, at all temperatures. Hence, we obtain in this case

$$\sigma = 1 - \frac{2}{x} \langle (S_\alpha^+ S_\alpha^-)_{av} \rangle. \quad (6.4)$$

The configurationally averaged spin-spin correlation  $\langle S_\alpha^+ S_\alpha^- \rangle$  can be expressed in terms of the density of states  $D(\Omega)$  and the Bose-Einstein distribution function  $f_{BE}(E)$  as

$$\begin{aligned} \langle (S_\alpha^+ S_\alpha^-)_{av} \rangle &= \sum_{\mathbf{k}} -\frac{1}{\pi} \text{Im} G_{\mathbf{k}\mathbf{k}}(\Omega) f_{BE}(2S\sigma x \Omega) \\ &= 2S\sigma x \int d\Omega D(\Omega) f_{BE}(2S\sigma x \Omega). \end{aligned} \quad (6.5)$$

This is an implicit equation for  $\sigma$  which has to be solved numerically. Results of  $\sigma$ , for several val-

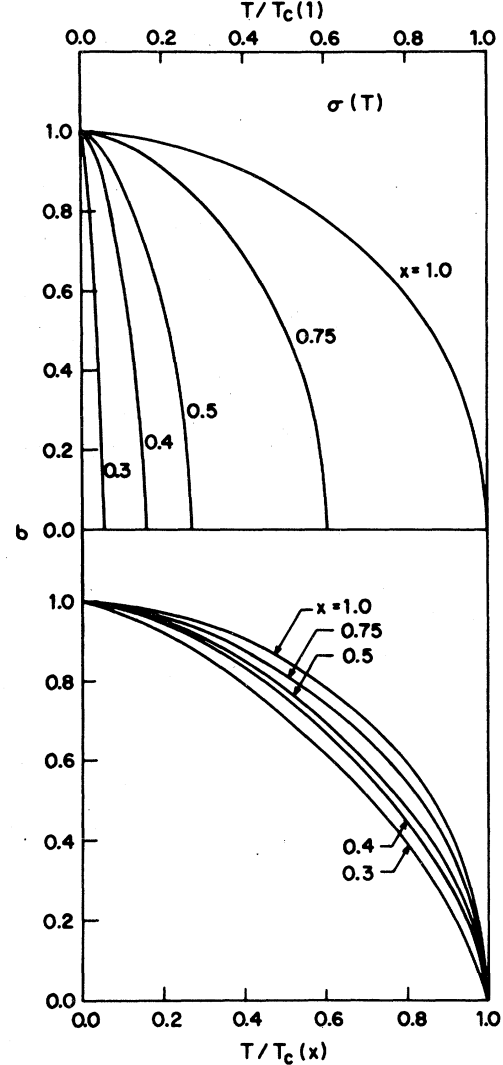


FIG. 20. Relative magnetization  $\sigma = M(T)/M(0)$  for several concentrations  $x$  plotted vs the reduced temperature  $T/T_c(1)$  and  $T/T_c(x)$ . For sc lattice.

ues of  $x$ , are presented in Fig. 20 as functions of the temperature  $T$  and the reduced temperature  $T/T_c(x)$ .

It can be seen that the values of  $\sigma(T)$  for various values of  $x$  do not fall on a single universal curve; the lower the concentration  $x$ , the more rapid is the decrease in  $\sigma(T)$ . This behavior was observed in experiments on nickel alloys,<sup>33,34</sup> amorphous CoP,<sup>35</sup> pseudobinary systems like  $\text{Gd}_x\text{Y}_{1-x}\text{Al}_2$ ,<sup>27</sup> and Fe alloys.<sup>36,37</sup> It should also be noted that  $\sigma(T)$ , in the absence of an external magnetic field, tends to zero at the critical concentration with an infinite slope. Similar results for  $\sigma(T)$  were obtained by Montgomery *et al.*<sup>24</sup> for a pure ferromagnet with random exchange interactions.

The thermal demagnetization at low temperature

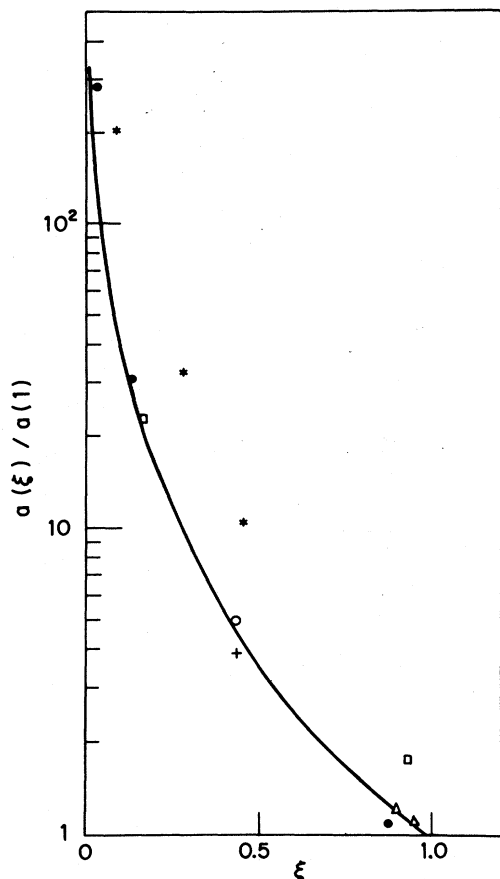


FIG. 21.  $a(x)$  of Eq. (5.6) plotted vs the reduced concentration  $\xi = (x - x_c)/(1 - x_c)$ . This is compared with experimental data:  $\text{Ni}_x\text{Cu}_{1-x}$ —full circles (Ref. 37),  $\text{Fe}_x\text{Sb}_{1-x}$ —triangles (Ref. 36),  $\text{Fe}_x\text{Au}_{1-x}$ —squares (Refs. 35, 36),  $\text{Ni}_x\text{Au}_{1-x}$ —stars (Ref. 29),  $\text{Gd}_x\text{Y}_{1-x}\text{Al}_2$ —crosses, and  $\text{Tb}_x\text{Y}_{1-x}\text{Al}_2$ —open circles (Ref. 28).

is found to obey the usual  $T^{3/2}$  law, namely,

$$\Delta\sigma = a(x)T^{3/2}, \quad (6.6)$$

where  $a(x) = [(x - x_c)/(1 - x_c)]^{-3/2}$  is strongly dependent on  $x$ . This is shown in Fig. 21.

When  $a(x)$  is plotted versus the reduced concentration  $\xi = (x - x_c)/(1 - x_c)$  (Fig. 8), it is found to be in quite good agreement with experimental results taken from various binary and pseudobinary alloys.<sup>38</sup> The agreement with the experimental results is somewhat surprising. First, since some of the data (e.g., Ni-Cu) are taken from systems which are itinerant ferromagnets, to which this model does not actually apply; second, the calculated  $a(x)$  refers to an sc lattice, which is not the case for all the data presented. The agreement, however, may indicate a universal dependence on the reduced concentration  $\xi$ .

The specific heat can be easily derived once the density of states has been calculated. We first ob-

tain results for the mean excitation energy

$$\bar{\omega}(x, T) = x\sigma(x, T) \int d\Omega \Omega D(\Omega) f_{\text{BE}}(2S\sigma x\Omega), \quad (6.7)$$

which for  $T = T_c(x)$  reduces to  $\bar{\omega}(x, T_c(x)) = \bar{\omega}_{\text{max}}(x) = J_1\beta_c(1)/\beta_c(x)$ . Since the number of excitations is normalized to  $2S\sigma x$  [cf. Eq. (5.4)] the total energy of the magnetic system is given by  $\bar{E} = 2S\sigma\bar{\omega}$ . The specific heat is then obtained by numerical differentiation. Results of  $C_V(T, x)$  for various values of  $x$  are shown in Fig. 22.

In specific-heat measurements of some  $A_xB_{1-x}$  alloys<sup>39,40</sup> (Ni-Pt, Ni-Cu) an anomalous peak was found near  $x_c$ . Two different schemes of analyzing this anomaly have been suggested: Robbins *et al.*<sup>40</sup> expressed  $C_V(T)$  as a sum of the electronic and phonon contributions ( $\gamma T + \alpha T^3$ ) and an additional, almost temperature-independent term which exhibits the  $x$ -dependent peak at  $x \sim x_c$ . Alternatively,<sup>41</sup>  $C_V$  was resolved as being composed of the phonon contribution  $\alpha T^3$  and enhanced  $\gamma(T)$   $T$  electronic contribution. It has also been suggested<sup>42,43</sup> that the anomalous contribution to the specific heat arises from spin excitation in finite magnetic clusters, which are abundant near  $x_c$ . Recalling our results of the density of states at  $x > x_c$ , it can be seen that low excitation energies become more dominant as  $x$  is decreased towards  $x_c$ . This has been interpreted as the contribution of spin-wave excitation within finite clusters. Following this reasoning, we have calculated  $C_V(x)$  at low temperatures for some values of  $T$ , using the previously calculated  $C_V(T)$ . Results are shown on Fig. 23. Clearly, as  $x$  approaches  $x_c$  from above,  $C_V(x)$  rises to a maximum at  $x_c$ . Although we have not carried out the calculation below  $x_c$ , it may however be assumed that  $C_V(x)$  would decrease since the cluster concentration decreases rapidly<sup>44</sup> as  $x$  is lowered.

#### ACKNOWLEDGMENT

We wish to thank Dr. D. Cabib for stimulating discussions.

#### APPENDIX

##### A. Calculation of $Q(\vec{k}, \Omega)$ and $P(\vec{k}, \Omega)$

The functions of  $P$  and  $Q$  in Eq. (2.18) are in an unsuitable form for numerical calculations. In this appendix,  $P$  and  $Q$  will be expressed in terms of a finite sum of products like  $f_i(\vec{k})C_i(\Omega)$ . The  $f_i$ 's are explicit real functions of  $\vec{k}$  and the  $C_i(\Omega)$ 's are lattice-structure-dependent, complex functions of  $\Omega$ , which can be calculated numerically.

We start with the function

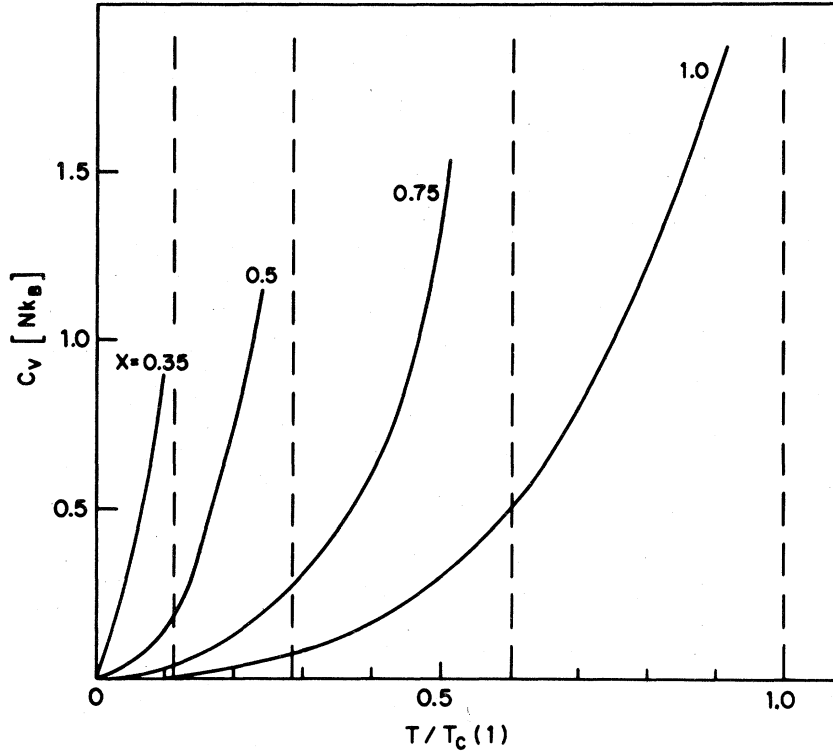


FIG. 22. Specific heat  $C_v$  plotted vs the reduced temperature  $T/T_c(1)$  for several concentrations  $x$ . For each concentration we dashed a vertical line at the corresponding critical temperature  $T_c(x)$ . For sc lattice.

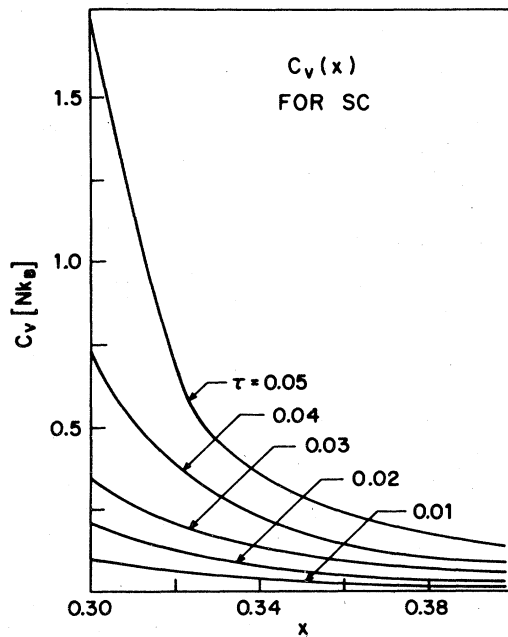


FIG. 23. Specific heat  $C_v$  vs concentration  $x$  for several low reduced temperatures  $T/T_c(1)$ . For sc lattice.

$$Q(\vec{k}, \Omega) = N^{-1} \sum_{\vec{q}} \frac{(J_{\vec{k}-\vec{q}} - J_{\vec{q}})(J_{\vec{k}-\vec{q}} - J_{\vec{k}})}{J_0 - J_{\vec{q}} - \Omega}, \quad (\text{A1})$$

where  $J_{\vec{k}} = \sum_{\vec{p}} J_{\vec{p}} e^{i\vec{k} \cdot \vec{p}}$ , being the lattice vectors, reduces to  $\sum_{\vec{p}} J_{\vec{p}} \cos \vec{k} \cdot \vec{p}$  due to the inversion symmetry of the cubic lattices.

Inserting this into Eq. (A1) one obtains

$$Q(\vec{k}, \Omega) = \sum_{\vec{p}, \vec{p}'} J_{\vec{p}} J_{\vec{p}'} [\Gamma_{\vec{p}}(\vec{k}) - \Gamma_{\vec{p}+\vec{p}'}(\vec{k})] \times [C_{\vec{p}}(\Omega) - C_{\vec{p}+\vec{p}'}(\Omega)] \quad (\text{A2})$$

where  $\Gamma_{\vec{p}}(\vec{k}) = 1 - \cos \vec{k} \cdot \vec{p}$ , and

$$C_{\vec{p}} = N^{-1} \sum_{\vec{q}} \frac{\Gamma_{\vec{p}}(\vec{q})}{J_0 - J_{\vec{q}} - \Omega}. \quad (\text{A3})$$

Note that  $C_{\vec{p}}(\Omega)$  depends only on the shell in which the lattice vector  $\vec{p}$  lies. It is thus convenient to express the sums in Eq. (A2) as sums over shells and over lattice vectors within the shells, i.e.,  $\sum_{\vec{p}} \rightarrow \sum_i \sum_{\vec{p}_i}$  where  $\vec{p}_i$  is a lattice vector in the  $i$ th shell. We thus obtain

$$Q(\vec{k}, \Omega) = \sum_{i,j} J_i J_j \left( \gamma_j(\vec{k}) z_i C_i(\Omega) - \frac{1}{z_j} \gamma_j(\vec{k}) \sum_m N_{ij}(m) z_m C_m(\Omega) + \sum_m N_{ij}(m) \gamma_m(\vec{k}) [C_m(\Omega) - C_i(\Omega)] \right) \\ \equiv \sum_i \varphi_i(\vec{q}) C_i(\Omega), \quad (A4)$$

where,  $C_i(\Omega) \equiv C_{\vec{p}_i}(\Omega) = z_i^{-1} \sum_q \gamma_i(q) / (J_0 - J_q - \Omega)$ ,  $z_i$  being the number of sites in the  $i$ th shell and  $\gamma_i(\vec{q}) = z_i^{-1} \sum_{\vec{p}_i} \Gamma_{\vec{p}_i}(q)$ .  $N_{ij}(m)$  is the number of times the  $m$ th shell is covered by all possible combinations of two successive steps, of order  $i$  and of order  $j$ . Values of  $N_{ij}(m)$  for the cubic lattices are given in Table II.

In the simplest cases, where only nn interactions are considered,  $Q$  reduces to

$$Q(\vec{k}, \Omega) = J_1 \left( z_1 C_1(\Omega) - \frac{1}{z_1} \sum_i n_i z_i C_i(\Omega) \gamma_1(\vec{k}) + \sum_i n_i C_i(\Omega) - C_1(\Omega) \gamma_1(\vec{k}) \right). \quad (A5)$$

Here we have defined  $n_i \equiv N_{11}(i)$ .

Similarly one obtains for  $P(\vec{k}, \Omega)$ ,

$$P(\vec{k}, \Omega) = \sum_i J_i [C_i(\Omega) - C_0(\Omega)] \gamma_i(\vec{k}), \quad (A6)$$

which, for nn interactions only, yields

$$P(\vec{k}, \Omega) = J_1 [C_1(\Omega) - C_0(\Omega)] \gamma_1(\vec{k}). \quad (A7)$$

$C_i(\Omega)$  at  $\Omega + i\delta$  is a complex function of  $\Omega$ , its imaginary part  $\text{Im}C_i(\Omega)$  is nonvanishing only in the interval  $0 < \Omega < (J_0 - J_{\vec{q}})_{\max}$  (for nn interactions only  $0 < \Omega < 2z_1 J_1$ ). We found it more convenient to calculate  $\text{Im}C_i(\Omega)$  which involves only a two-dimensional integral over a cross section of the Brillouin zone) and then obtained  $\text{Re}C_i(\Omega)$  by use of the Kramers-Kronig relation,

$$\text{Re}C_i(\Omega) = \frac{1}{\pi} P \int_0^{(J_0 - J_{\vec{q}})_{\max}} \frac{\text{Im}C_i(\Omega')}{(\Omega - \Omega')} d\Omega'. \quad (A8)$$

The numerical results were checked against "sum rules" which the  $C_i$ 's have to satisfy. The sum rules are as follows:

Consider the expression:

$$N^{-1} \sum_{\vec{q}} \frac{J_0 - J_{\vec{q}}}{J_0 - J_{\vec{q}} - \Omega} = \sum_i J_i z_i C_i(\Omega). \quad (A9)$$

Subtracting and adding  $\Omega$  to the numerator, under the  $\vec{q}$  sum, one obtains

$$\sum_i J_i z_i C_i(\Omega) - \Omega C_0(\Omega) = 1, \quad (A10)$$

which, for nn interactions only, reduced to

$$J_1 z_1 C_1(\Omega) - \Omega C_0(\Omega) = 1. \quad (A11)$$

Similarly, by direct calculation of the expression  $N^{-1} \sum (J_0 - J_{\vec{q}})^2 / (J_0 - J_{\vec{q}} - \Omega)$  and then by subtracting and adding  $\Omega^2$  to the numerator under the  $\vec{q}$  sum, one obtains

$$\sum_{i,j} J_i J_j \left( 2z_i z_j C_i(\Omega) - \sum_m N_{ij}(m) z_m C_m(\Omega) \right) \\ = \sum_i J_i z_i + \frac{\Omega}{J_1} + \left( \frac{\Omega}{J_1} \right)^2 C_0(\Omega), \quad (A12)$$

which, for nn interactions only, reduces to

$$\frac{1}{z_1} \left\{ \sum_i n_i z_i C_i(\Omega) + \frac{\Omega}{J_1} \left[ 1 + \left( \frac{\Omega}{J_1} - 2z_1 \right) C_0(\Omega) \right] \right\} = 1. \quad (A13)$$

Equations (A10) and (A12) produce *four* sum rules (both for  $\text{Re}C_i$  and  $\text{Im}C_i$ ). In all the stages of the calculation, we ensured that these were satisfied. The  $C_i$ 's were computed for  $\Omega \neq 0$  with nn interactions only and for  $\Omega = 0$  including second-neighbors of relative strength  $\eta$ . These were denoted in Sec. IV by  $C_i(\eta)$ .

#### B. Numerical calculation of $Q_H$ and $P_H$

$P_H$  and  $Q_H$  may be easily shown to satisfy equations like (A4) and (A6), with  $\gamma_i$  defined as before. The  $C_i$ 's (from now on  $C_i^H$ ), however, satisfy the following integral equation:

$$C_i^H = \sum_{\vec{q}} (1 - \cos \vec{k} \cdot \vec{p}_i) \\ \times \left( \Omega - (J_0 - J_{\vec{q}}) + \frac{1-x}{x} \sum_j f_j(\vec{q}) C_j^H \right)^{-1} \quad (A14)$$

where the  $f_j(\vec{q})$  are the same functions defined by Eq. (A4).

Clearly, the  $C_i^H$  are no longer  $x$  independent as was the case with the old  $C_i$ . It is also obvious from (A14) that at  $\Omega$  large enough  $C_i^H \rightarrow C_i$ . We therefore solved Eq. (A14), for fixed  $x$ , by iteration starting from large  $\Omega$  and with  $C_i^{H(0)} = C_i$ . Convergence problems arose only at  $x$  close enough to  $x_c$ .

- \*In partial fulfillment of the requirements for the degree of D. Sc. at the Dept. of Physics, Technion, Haifa, Israel.
- <sup>1</sup>R. Brout, Phys. Rev. 115, 824 (1959).
  - <sup>2</sup>H. Sato, A. Arrott, and R. Kikuchi, J. Phys. Chem. Solids 10, 19 (1959).
  - <sup>3</sup>J. S. Smart, J. Phys. Chem. Solids 16, 169 (1960).
  - <sup>4</sup>R. J. Elliott and B. R. Heap, Proc. R. Soc. A 265, 264 (1962).
  - <sup>5</sup>R. J. Elliott, J. Phys. Chem. Solids 16, 165 (1960).
  - <sup>6</sup>S. H. Charap, Phys. Rev. 126, 1393 (1962).
  - <sup>7</sup>P. G. de Gennes, P. Lafore, and P. Millot, J. Phys. Chem. Solids 11, 105 (1959).
  - <sup>8</sup>P. G. de Gennes, P. Lafore, and P. Millot, J. de Phys. Radium 20, 624 (1959).
  - <sup>9</sup>R. J. Elliott, B. R. Heap, D. J. Morgan, and G. S. Rushbrooke, Phys. Rev. Lett. 5, 366 (1960).
  - <sup>10</sup>C. Domb and M. F. Sykes, Phys. Rev. 122, 77 (1961).
  - <sup>11</sup>M. F. Sykes and J. W. Essam, Phys. Rev. 133, A310 (1964).
  - <sup>12</sup>G. S. Rushbrooke and D. J. Morgan, Mol. Phys. 4, 1 (1961).
  - <sup>13</sup>D. J. Morgan and G. S. Rushbrooke, Mol. Phys. 6, 477 (1963).
  - <sup>14</sup>G. A. Murray, Proc. Phys. Soc. Lond. 111, 89 (1966).
  - <sup>15</sup>D. Kumar and A. B. Harris, Phys. Rev. B 8, 2166 (1973).
  - <sup>16</sup>T. Kaneyoshi, Progr. Theor. Phys. 42, 477 (1969).
  - <sup>17</sup>S. F. Edwards and R. C. Jones, J. Phys. C 4, 2109 (1971).
  - <sup>18</sup>R. A. Tahir-Kheli, Phys. Rev. B 6, 2808 (1972).
  - <sup>19</sup>R. J. Elliott and D. E. Pepper, Phys. Rev. B 8, 2374 (1973).
  - <sup>20</sup>A. B. Harris, P. L. Leath, B. G. Nickel, and R. J. Elliott, J. Phys. C 7, 1963 (1974).
  - <sup>21</sup>W. H. Butler and W. Kohn, J. Res. Natl. Bur. Stand. A 74, 443 (1970).
  - <sup>22</sup>A. Theumann and R. A. Tahir-Kheli, Phys. Rev. B 12, 1796 (1975).
  - <sup>23</sup>B. G. Nickel, J. Phys. C 8, 1719 (1974).
  - <sup>24</sup>Yu. Izyumov, Proc. Phys. Soc., Lond. 87, 505 (1966).
  - <sup>25</sup>C. G. Montgomery, J. I. Kruger, and R. M. Stubbs, Phys. Rev. Lett. 25, 669 (1970).
  - <sup>26</sup>D. N. Zubarev, Sov. Phys.-Usp. 3, 320 (1960).
  - <sup>27</sup>J. Danan *et al.*, Conference on Rare Earth and Activities, Durham, England, 1971 (unpublished).
  - <sup>28</sup>K. H. J. Buschow, J. F. Fast, A. M. van Diepen, and H. W. de Wijn, Phys. Status Solidi 24, 715 (1967).
  - <sup>29</sup>P. Le Cocq, Ann. Chim. 8, 85 (1963).
  - <sup>30</sup>V. K. S. Shante and S. Kirkpatrick, Adv. Phys. 20, 325 (1971).
  - <sup>31</sup>S. Kirkpatrick, Solid State Commun. 12, 1279 (1973).
  - <sup>32</sup>M. F. Sykes, D. S. Gaunt, and M. Glen, J. Phys. A 9, 1805 (1976).
  - <sup>33</sup>S. A. Ahern, M. J. C. Martin, and W. Sucksmith, Proc. R. Soc. Lond. 248, 145 (1958).
  - <sup>34</sup>J. R. Clinton, E. H. Tyler, and H. L. Lou, J. Phys. F 4, 1162 (1974).
  - <sup>35</sup>R. W. Cochrane and G. S. Cargill III, Phys. Rev. Lett. 32, 486 (1974).
  - <sup>36</sup>E. Scheil, H. Specht, and E. Wachtel, Z. Metallkd. 49, 590 (1958).
  - <sup>37</sup>A. J. Aldred, J. Phys. C 1, 1103 (1968).
  - <sup>38</sup>V. E. Rode, A. Blyushke, A. Finkel'berg, and A. I. Leichenko, Sov. Phys.-JETP 35, 568 (1972).
  - <sup>39</sup>J. Beille, D. Bloch, and R. Kuentzler, Solid State Commun. 14, 963 (1974).
  - <sup>40</sup>C. G. Robbins, H. Claus, and P. A. Beck, J. Appl. Phys. 40, 2269 (1969).
  - <sup>41</sup>K. H. Bennemann, Phys. Rev. 167, 564 (1968).
  - <sup>42</sup>K. Schröder, J. Appl. Phys. 32, 880 (1961).
  - <sup>43</sup>E. J. Hayes, A. Hahn, and E. P. Wohlfarth, J. Phys. F 2, 351 (1972).
  - <sup>44</sup>H. Dvey-Aharon and M. Fibich, Phys. Rev. B 10, 287 (1974).